Three-Dimensional Solution NMR Structure of Apo-L75F-TrpR, a Temperature-Sensitive Mutant of the Tryptophan Repressor Protein†

Robert Tyler,‡ István Pelczer,§ Jannette Carey,§ and Valérie Copié*,‡

Department of Chemistry and Biochemistry, Montana State University, 108 Gaines Hall, Bozeman, Montana 59717, and Department of Chemistry, Princeton University, Princeton, New Jersey 08544-1009

Received April 24, 2002

ABSTRACT: L75F-TrpR is a temperature-sensitive mutant of the tryptophan repressor protein of *Escherichia coli* in which surface-exposed residue leucine 75 in the DNA binding domain is replaced with phenylalanine. Biochemical and biophysical studies had suggested global alterations in dynamics for L75F-TrpR, although the structure was apparently similar to that of wild-type TrpR. Herein, we report the three-dimensional solution structure of apo-L75F-TrpR determined by multidimensional (^{1}H, ^{15}N, and ^{13}C) solution NMR spectroscopy. An ensemble of structures was generated from 769 unique NOE-based distance restraints, 68 dihedral angle restraints, and 62 hydrogen bond distance restraints. Apo-L75F-TrpR exhibits a three-dimensional (3D) fold very similar to that of apo-WT-TrpR, with a dimeric core of four α-helices (A−C and F) from each subunit, and less well-defined D and E helical regions of the DNA binding domains. Despite their many similarities, wild-type and mutant proteins display significant chemical shift differences, one cluster of which is in the B−C turn, too distant to be ascribed solely to ring current effects from Phe75. Differences in NOE patterns and amide proton exchange rates are also observed in the B−C turn region. The data provide evidence that this point mutation exerts local effects on structure and stability in the DNA binding domain, and propagates long-range effects through the tertiary structure.

The tryptophan repressor protein (TrpR)[1] of *Escherichia coli* has been the focus of extensive structural and biological study. Much of this effort has been devoted to elucidating the mechanism(s) by which changes in the protein's three-dimensional (3D) structure and/or its conformational flexibility modulate the biological activity of the repressor. The TrpR protein is comprised of two identical 108-residue polypeptide chains and forms a symmetric 25 kDa dimer (*1*). The apo form of TrpR (apo-WT-TrpR) binds two molecules of L-tryptophan (L-Trp) to form a holorepressor, which in turn binds to specific DNA operator sequences. Extensive structural studies by both X-ray (*2*, *3*) and NMR (*4*−*6*) have shown that this protein is comprised of six α-helices per monomer (A−F). Helices A−C and F of two monomers together form the hydrophobic core of the TrpR dimer, while helices D and E form the helix−turn−helix DNA binding domain. TrpR's primary function is to regulate genes whose expression controls intracellular levels of tryptophan (for a review, see ref *7*). In the presence of high concentrations of L-Trp in the cell, the holo-TrpR protein inhibits expression of several genes that are responsible for the uptake and biosynthesis of tryptophan.

In solution, both apo- and holo-TrpR have tertiary folds similar to those found in the corresponding crystal structures (*2*−*6*). The NMR solution structures reveal, however, that the DNA binding domain is more flexible and disordered than in the crystal structures (*5*, *8*−*10*). In particular, Jardetzky, Arrowsmith, and co-workers have shown that helices D and E are highly dynamic in apo-TrpR, and that binding of the corepressor L-Trp is correlated with the presence of additional intrahelical ^{1}H−^{1}H NOE connectivities within the helix E region of the holorepressor that are not observed in apo-TrpR (*5*), and by the observations of slower backbone amide proton ^{1}H−^{2}H exchange rates and changes in NMR relaxation time constants (*8*−*11*). Similar effects are observed for helix D when holo-trpR binds to the DNA operator (*6*).

Mutational studies with TrpR reveal that the flexibility and structural ordering of the DNA binding domain can be perturbed by modest changes in the amino acid sequence, and lead to altered function. For example, the mutant in which alanine 77 is replaced with valine displays reduced dynamics (*12*, *13*) and increased helical order in the apoprotein DNA binding region (*14*), and leads to differential binding of holo-TrpR to closely related DNA operator sequences (*15*). Temperature-sensitive (ts) mutants have the potential to yield additional insights about the relationship between TrpR structure, stability, and dynamics. Extensive biophysical and biochemical characterization of the TrpR ts

† This work was funded in part by NSF Career Grant MCB-9984562 to V.C. and NSF Grant MCB98-14117 to J.C.

* To whom correspondence should be addressed. E-mail: vcopie@chemistry.montana.edu. Phone: (406) 994-7244. Fax: (406) 994-5407.

‡ Montana State University.

§ Princeton University.

[1] Abbreviations: TrpR, tryptophan repressor; apo-WT-TrpR, wild-type aporepressor; apo-L75F-TrpR, L75F mutant aporepressor; L-Trp, L-tryptophan; NMR, nuclear magnetic resonance; NOE, nuclear Overhauser effect; NOESY, nuclear Overhauser effect spectroscopy; 2D ^{1}H−^{15}N HSQC and HSQC, heteronuclear single-quantum coherence; CSI, chemical shift indexing; DSS, 2,2-dimethyl-2-silapentane-5-sulfonic acid; CNS, Crystallography and NMR System; NCS, noncrystallographic symmetry; rmsd, root-mean-square deviation; 1σ, one standard deviation.

10.1021/bi020304t CCC: $22.00
Published on Web 09/11/2002

mutant L75F in which leucine 75 is replaced with phenylalanine (*16*) has revealed that the apoprotein displays an increase in α-helicity as measured by CD, a more buried environment for one or both intrinsic tryptophan residues (Trp19 and Trp99), and slower proton−deuterium exchange rates for their spectrally resolved indole ring protons, but displays little apparent difference in either overall tertiary structure or stability compared to WT-TrpR. These data suggested that this conservative mutation of a surface-exposed residue generates nonlocal effects throughout the protein (*16*). To understand this effect, we have undertaken structural and dynamic studies of L75F-TrpR in solution.

Here, we report the three-dimensional solution structure of dimeric apo-L75F-TrpR. The protein structure was determined using heteronuclear (^{1}H, ^{15}N, and ^{13}C) multidimensional solution NMR methods. Structural calculations were performed using both Crystallography and NMR (CNS) (*17*) and X-PLOR 3.1 (*18*) software. Determination of the 3D structure of the L75F dimer was based on the following set of uniquely determined restraints: 769 NOE-derived distance restraints, 68 dihedral angle restraints, and 62 hydrogen bond distance restraints. The structural calculations resulted in an ensemble of 20 lowest-energy conformers, with an average root-mean-square deviation (rmsd) of 1.0 Å for backbone atoms in the core helices A−C and an average rmsd value of 2.8 Å for backbone atoms in the D−E chain segment, residues 67−92. The NMR results support the earlier finding that this mutation indeed propagates long-range effects throughout the protein. Our solution structure suggests that sections of helices D and E are more structured in apo-L75F-TrpR than in apo-WT-TrpR (*4*, *5*). We also report significant ^{1}H and ^{15}N chemical shift changes, compared to apo-WT-TrpR, for backbone amides distant from the site of mutation in apo-L75F. Our analyses suggest that ring current shifts originating from the new phenylalanine side chain cannot account solely for some chemical shift changes. These chemical shift differences and other differences detected by NMR, together with inspection of the ensemble of apo-L75F-TrpR structures, point to a reordering of the protein structure near the L-Trp binding pocket.

MATERIALS AND METHODS

Sample Preparation. E. coli strains CY15071 and CY15075 and the plasmid pJPR2.L75F are as described by Jin et al. (*16*). Uniformly ^{15}N- or ^{15}N- and ^{13}C-enriched L75F-TrpR protein was isolated from CY15071 or CY15075 transformed with the overproducing plasmid pJPR2.L75F. The strains were grown in M9 minimal medium enriched with [^{15}N]NH_4Cl (99% ^{15}N-enriched, CIL, Cambridge, MA) or [^{15}N]NH_4Cl/[$^{13}C_6$]-D-glucose (99% ^{13}C-enriched, CIL) as the sole nitrogen and carbon sources, respectively. Protein purification procedures were carried out as described by Jin et al. (*16*). The CY15071 cell cultures were supplemented with 20 mL of a 0.2 M unlabeled threonine stock solution per liter because this strain of *E. coli* cannot synthesize threonine de novo. Protein samples made from CY15071 bacterial cell growths lacked ^{15}N- or ^{15}N- and ^{13}C-labeled threonine residues, and as a result, the threonines from these protein samples were unobservable in the heteronuclear multidimensional NMR experiments. Uniformly labeled protein, containing ^{15}N- or ^{15}N- and ^{13}C-labeled threonines, was produced by overexpressing the L75F-TrpR protein in strain CY15075 grown in M9 minimal medium supplemented with [^{15}N]ammonium chloride and $^{13}C_6$-labeled glucose. This strain also produces a low level of WT-TrpR from the chromosome. The ^{15}N-labeled wild-type aporepressor protein, used for comparison, was graciously donated by E. Hyde and R. Parslow. Protein samples were concentrated to 1−2 mM protein dimer in NMR buffer (500 mM NaCl, 50 mM NaH_2PO_4, and 90% H_2O/10% D_2O) at pH 5.7.

NMR Spectroscopy. All NMR spectra were acquired at 45 °C on a four-channel Bruker DRX-600 spectrometer, with a triple ^{15}N, ^{13}C, ^{1}H inverse resonance probe equipped with triple-axis gradients. Quadrature detection for all multidimensional NMR experiments was achieved by recording the data in States−TPPI mode in the indirect dimensions (*19*). ^{1}H and ^{13}C dimensions were referenced to DSS, while the ^{15}N dimension was referenced to $^{15}NH_4Cl$. A detailed description of all experimental NMR parameters is provided in Table S1 of the Supporting Information. All data were processed and analyzed using NMRPipe (*20*), PIPP (*21*), and Xwinnmr (Bruker Inc.) software packages. Strip plots of the 3D ^{15}N-edited ^{1}H−^{1}H NOESY spectrum were made using the *plot_sequence* software generously provided to us by D. Garrett of the National Institutes of Health (Bethesda, MD).

Two-dimensional ^{1}H−^{15}N HSQC (*22*) spectra were acquired with spectral widths of 12.0 ppm in t_2 and 30.0 ppm in t_1, with the proton carrier frequency set at 4.7 ppm and the nitrogen carrier set at 115.5 ppm. Data were collected with 1024 complex points in t_2 and 128 complex points in t_1, using Waltz-16 (*23*) for ^{15}N decoupling during data acquisition. Apodization was performed using a sine bell squared function shifted by 0.35 π radians in t_2, and a sine bell function shifted by 0.40 π radians in t_1.

Sequential ^{1}H and ^{13}C backbone and side chain chemical shift assignments were extracted from a series of heteronuclear three-dimensional NMR experiments [HNCACB, CBCA(CO)NH, C(CO)NH, HBHA(CO)NH, and HC(CO)NH] (*24*−*27*), acquired with spectral widths of 12.0 (in t_3), 67.0 (in t_2), and 30.0 ppm (in t_1) for the proton, carbon, and nitrogen spectral dimensions, respectively. Proton and nitrogen carrier frequencies were set to the same values described for the two-dimensional (2D) ^{1}H−^{15}N HSQC experiment, with the additional carbon carrier frequency set to 46.0 ppm in the 3D experiments. Data were collected with 512, 58, and 24 complex points in t_3, t_2, and t_1, respectively, using the DIPSI scheme (*28*) for ^{1}H decoupling during carbon evolution, and the Waltz-16 scheme for ^{15}N decoupling during data acquisition. Similar apodization functions were used in all spectral dimensions, using shifted sine bell functions.

Structure Calculations. A large portion of the NOE-based distance restraints for the structure calculations were derived from 3D ^{15}N-edited ^{1}H−^{1}H NOESY (*29*, *30*) experiments recorded with NOE mixing periods of 50, 90, and 120 ms. Additional NOE connectivities to aliphatic protons were identified from a 3D ^{13}C-edited ^{1}H−^{1}H NOESY experiment (*31*) recorded with a NOE mixing time period of 120 ms. A total number of 730 NOE cross-peaks were assigned per monomer, and along with 39 intermonomer assignments served as the basis for the calculations of the three-dimensional structure of apo-L75F-TrpR in solution. NOE

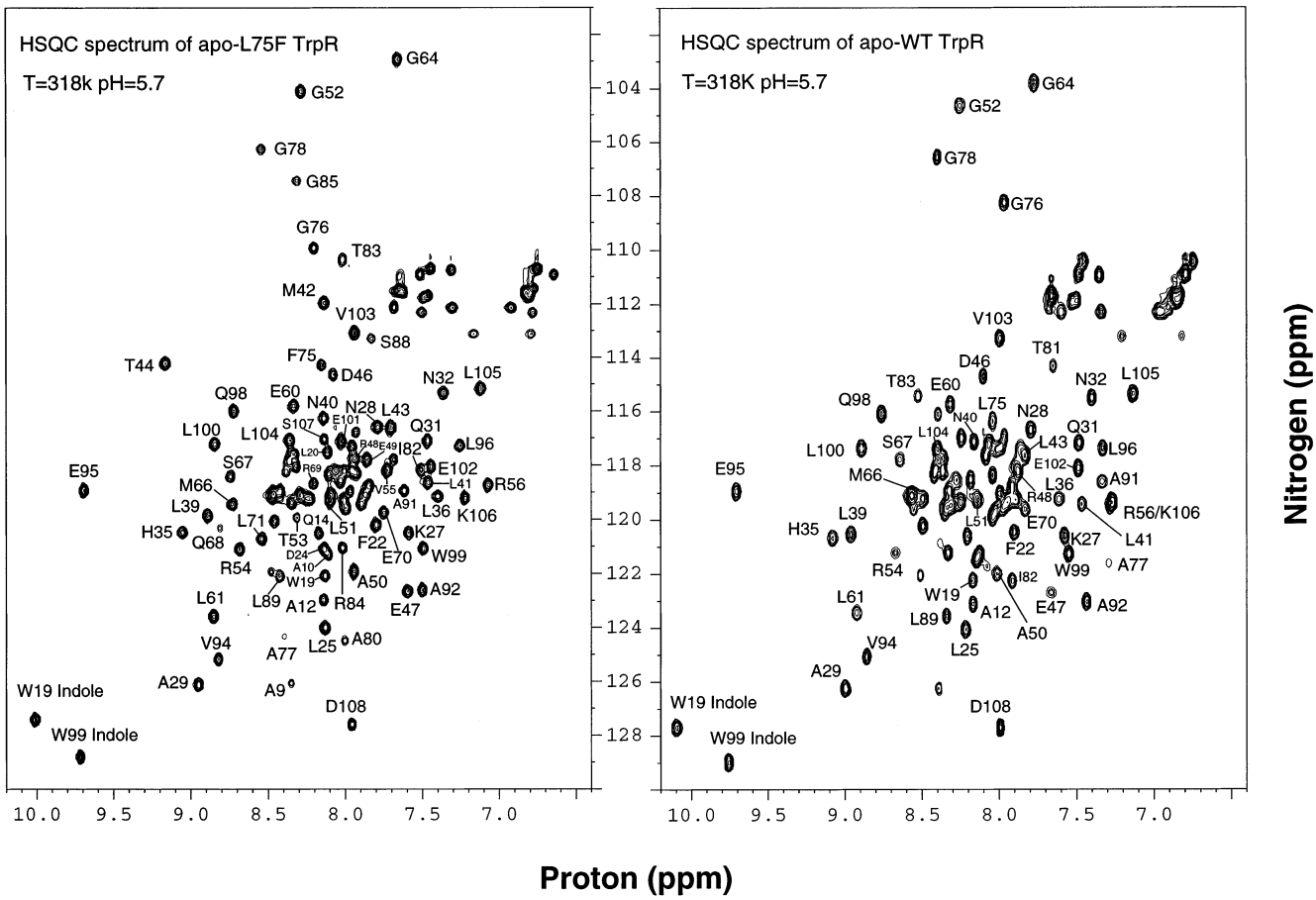

FIGURE 1: 2D $^{1}H-^{15}N$ HSQC spectra. Spectra of uniformly ^{15}N-labeled apo-L75F-TrpR and apo-WT-TrpR were recorded at 45 °C in 500 mM NaCl, 50 mM Na_2HPO_4, and 90% H_2O/10% D_2O at pH 5.7. Some residue labels are omitted for clarity. The cluster of unlabeled cross-peaks at 7.0−8.0/110−114 ppm arises from side chain NH_2 resonances. Resonances for Thr44, Arg84, Gly85, and Ser88 are not observed in the spectrum of apo-WT-TrpR under these solution conditions.

cross-peaks were classified into four categories, and restraints were given the following ranges based on the qualitative analyses of the NOE cross-peak intensities: strong (1.8−3.0 Å), medium (1.8−3.5 Å), weak (1.8−4.5 Å), and very weak (1.8−5.0 Å). Hydrogen bonding distance restraints were identified through $^{1}H-^{2}H$ amide exchange experiments, and were given boundaries of 1.5−2.3 (H−O) and 2.5−3.3 Å (N−O). Due to the extensive α-helical content of the TrpR protein and significant overlap of spectral resonances, three bond H_N-H_α scalar couplings could not be measured reliably. However, following the seminal work of Zhao et al. (*5*), $^{1}H_\alpha$ and $^{13}C_\alpha$ chemical shift indexing and NOE patterns characteristic of secondary structural elements were used to conservatively restrict ϕ torsion angles to $-65 \pm 45°$ for the hydrophobic core helices (A−C and F) and to $-65 \pm 60°$ for the helix−turn−helix region (D and E).

Simulated annealing was performed on two identical monomeric extended structures, spanning residues 3−108, using the program Crystallography and NMR systems, version 1.0 (CNS) (*16*). Forty structures were calculated using the standard input file *anneal.inp* modified to include 4000 steps for both the high-temperature and the first slow-cooling annealing stage in torsion angle space. The molecular dynamic scheme used in CNS followed standard protocols (*17*, *32*), and consisted of the following stages: (a) heating in torsion angle space at 50 000 K for 60 ps with the energy constant for the van der Waals parameters scaled by 0.1, (b) cooling in torsion angle space to 2000 K for 60 ps with ramping of the van der Waals parameters to full scale, (c) cooling in Cartesian space to 300 K for 15 ps using conventional molecular dynamics, and (d) 2000 steps of conjugate-gradient Powell minimization. The weights for the NOE restraints were set to 150 kcal/mol for stages a−c and 75 kcal/mol for stage d. The functional form of the NOE distance restraints was a flat-bottomed parabolic function with a soft asymptote. A sum averaging function was used for both NOE and H-bond restraints. The weights of the dihedral angle restraints were set to 100 kcal/mol for stage a, 200 kcal/mol for stages b and c, and 400 kcal/mol for the final stage (d).

The 40 calculated structures were further refined against noncrystallographic symmetry (NCS) restraints using the X-PLOR program, version 3.1 (*18*). This computational step was undertaken to ensure 2-fold symmetry of the final L75F-TrpR dimer structures, which is reflected in the unique set of $^{1}H-^{15}N$ resonances observed in the 2D $^{1}H-^{15}N$ HSQC spectrum of apo-L75F-TrpR. NCS weighting factors were set to 25 kcal mol^{-1} $Å^{-2}$ for all backbone atoms and 5 kcal mol^{-1} $Å^{-2}$ for all other non-hydrogen atoms. The 20 lowest-energy structures were then selected and analyzed using the programs Quanta (Molecular Simulations Inc.), Procheck NMR (*33*), MOLMOL (*34*), and DisCal (A. Hinck, unpublished). Calculations of average and pairwise rmsds were performed in X-PLOR using the program's standard *average.inp* and *rms_pairwise.inp* scripts (*18*).

RESULTS AND DISCUSSION

Resonance assignments for apo-L75F-TrpR were determined using standard methods applied previously to WT-TrpR, and several backbone amide assignments for apo-WT-TrpR were also confirmed independently in this work. The 2D $^{1}H-^{15}N$ HSQC correlation spectra of the two proteins recorded under identical temperature, pH, and buffer conditions are shown in Figure 1. Consistent with the spectra that are shown, the subunit assembly state of apo-L75F-TrpR in solution is primarily dimeric, with only very minor higher-order aggregation similar to that of apo-WT-TrpR under equivalent conditions (R. Fairman, personal communication, 2001). Thus, as reported previously (*16*), the two proteins have very similar overall structures, although differences in cross-peak number and resonance frequency (Table 1) are evident in the spectra of Figure 1.

Using a combination of 2D and 3D heteronuclear NMR experiments (complete list available as Table S1 of the Supporting Information), the backbone and side chain resonances of apo-L75F-TrpR were assigned. Of the 107 peptide groups, and excluding the four prolines of each apo-L75F-TrpR monomer, 102 of their $^{15}N-^{N}H$ resonances and 105 of their $^{13}C_{\alpha}$ resonances could be assigned unambiguously, as well as H_{α} protons of 105 residues, and a majority of side chain ^{13}C and ^{1}H resonances. A complete list of chemical shift assignments is available in the Supporting Information (Table S2). NOE cross-peaks were assigned to intermonomer connectivities only after all other possible identifications were ruled out, as described below.

Regions of secondary structure within apo-L75F-TrpR were evaluated using a combination of the chemical shift index (CSI) for $^{1}H_{\alpha}$ and $^{13}C_{\alpha}$ (*35*−*37*), NOE-based short- and medium-distance estimates, and $^{1}H-^{2}H$ exchange information. The results are summarized in Figure 2. As expected for an all-helical protein, and as found previously for WT-TrpR (*4*, *5*), the patterns that are shown reflect the presence of well-defined helices encompassing chain segments corresponding to helices A−C and F. Chain segments corresponding to helices D and E show some, though less strong or complete, indications of helical character. However, compared to previously published NOE assignments of apo-WT-TrpR (see Figure 1 of ref *5*), the chain segment of residues 67−92 of apo-L75F-TrpR exhibits more pronounced helical chemical shift indices, and displays a larger number of NOE connectivities, although this D−E region still lacks many of the longer-range NOEs characteristic of well-formed helices, such as the $d_{N}\alpha(i, i+3)$ NOEs. Figure 3 displays a portion of the ^{15}N-edited $^{1}H-^{1}H$ NOESY spectrum of apo-L75F-TrpR reconstructed to present sequential backbone amide NOE strips for residues 71−82. The data include a number of strong, well-developed sequential and intraresidue cross-peaks for residues in this chain segment. Many of the NOE cross-peaks are unique to the L75F mutant due to the Phe75 side chain. A direct comparison with the ^{15}N-edited spectral region of apo-WT-TrpR proved to be inconclusive due to extensive resonance overlaps of corresponding residues in the 3D ^{15}N-edited $^{1}H-^{1}H$ NOESY spectrum of apo-WT-TrpR recorded under identical conditions (data not shown).

A total of 769 uniquely identified NOE restraints (1538 for the symmetric dimer) were used to calculate the three-dimensional structure of apo-L75F-TrpR in solution. Potential intermonomer contacts were identified with the aid of previously published WT-TrpR NMR structures (*4*, *5*), and the corresponding NOEs in our data were evaluated first in preliminary calculated structures of apo-L75F-TrpR and then iteratively in progressively refined structures. Twenty-five of the 39 intermonomer NOEs used in the structure calculations were derived from very well-resolved regions of the

Table 1: ^{1}H and ^{15}N Amide Chemical Shift Changes between L75F- and WT-TrpR Apoproteins[a]

residue	$\Delta^{1}H_{N}$ (ppm)	$\Delta^{15}N$ (ppm)	residue	$\Delta^{1}H_{N}$ (ppm)	$\Delta^{15}N$ (ppm)
Met1	na	na	Val55	−0.15	−0.69
Ala2	na	na	Arg56	−0.18	−0.68
Gln3	na	na	Ile57	−0.25	1.14
Gln4	na	na	Val58	−0.01	na
Ser5	na	na	Glu59	0.00	−0.04
Pro6	na	na	Glu60	0.05	0.08
Tyr7	na	na	Leu61	0.01	0.24
Ser8	na	na	Leu62	−0.02	−0.42
Ala9	na	na	Arg63	0.15	na
Ala10	na	na	Gly64	−0.08	−0.78
Met11	na	na	Glu65	0.04	na
Ala12	na	na	Met66	0.22	0.38
Glu13	na	na	Ser67	0.03	0.95
Gln14	na	na	Gln68	1.03	0.86
Arg15	na	na	Arg69	−0.02	0.22
His16	0.03	0.21	Glu70	−0.22	−0.08
Gln17	0.00	−0.09	Leu71	−0.34	na
Glu18	0.01	−0.07	Lys72	na	na
Trp19	0.03	−0.95	Asn73	0.13	−1.32
Leu20	0.07	−0.15	Glu74	−0.49	−0.91
Arg21	na	na	Phe75	−	−
Phe22	−0.04	−0.21	Gly76	0.32	1.75
Val23	0.07	−1.67	Ala77	1.01	1.44
Asp24	0.06	−0.36	Gly78	0.23	−0.17
Leu25	0.03	0.11	Ile79	na	na
Leu26	0.00	−1.56	Ala80	na	na
Lys27	0.07	0.04	Thr81	0.10	−2.03
Asn28	0.05	−0.08	Ile82	−0.36	−3.90
Ala29	0.03	0.00	Thr83	−0.47	−4.42
Tyr30	0.03	−1.92	Arg84	na	na
Gln31	0.03	−0.03	Gly85	na	na
Asn32	0.01	−0.26	Ser86	na	na
Asp33	0.05	−0.06	Asn87	0.57	na
Leu34	0.03	0.10	Ser88	na	na
His35	0.00	−0.16	Leu89	0.11	−1.30
Leu36	−0.04	−0.25	Lys90	0.13	0.00
Pro37	−	−	Ala91	0.31	0.36
Leu38	−0.15	−0.26	Ala92	0.16	−0.28
Leu39	−0.03	−0.62	Pro93	−	−
Asn40	−0.08	−0.69	Val94	0.01	0.14
Leu41	−0.08	−0.68	Glu95	0.03	−0.01
Met42	0.02	−1.17	Leu96	−0.01	−0.05
Leu43	−0.15	−1.03	Arg97	0.09	−0.12
Thr44	0.05	−1.21	Gln98	0.00	0.01
Pro45	−	−	Trp99	0.00	−0.18
Asp46	0.02	0.10	Leu100	−0.01	−0.13
Glu47	−0.02	0.26	Glu101	0.03	−0.17
Arg48	0.10	−0.46	Glu102	0.01	−0.03
Glu49	0.06	0.15	Val103	−0.01	−0.29
Ala50	−0.01	0.10	Leu104	−0.01	−0.25
Leu51	0.00	−0.22	Leu105	−0.04	−0.23
Gly52	0.05	−0.49	Lys106	0.01	−0.05
Thr53	0.07	na	Ser107	na	na
Arg54	0.04	−0.49	Asp108	0.03	0.00

[a] Chemical shift changes are defined as Δ (ppm) = apo-L75F-TrpR − apo-WT-TrpR. Chemical shift values for apo-WT-TrpR are taken from refs *8* and *11*, corrected when necessary for differences in chemical shift referencing, except for Gly78 (taken from Figure 1 of this work). na means that chemical shifts for apo-WT-TrpR are not available for comparison with apo-L75F-TrpR.

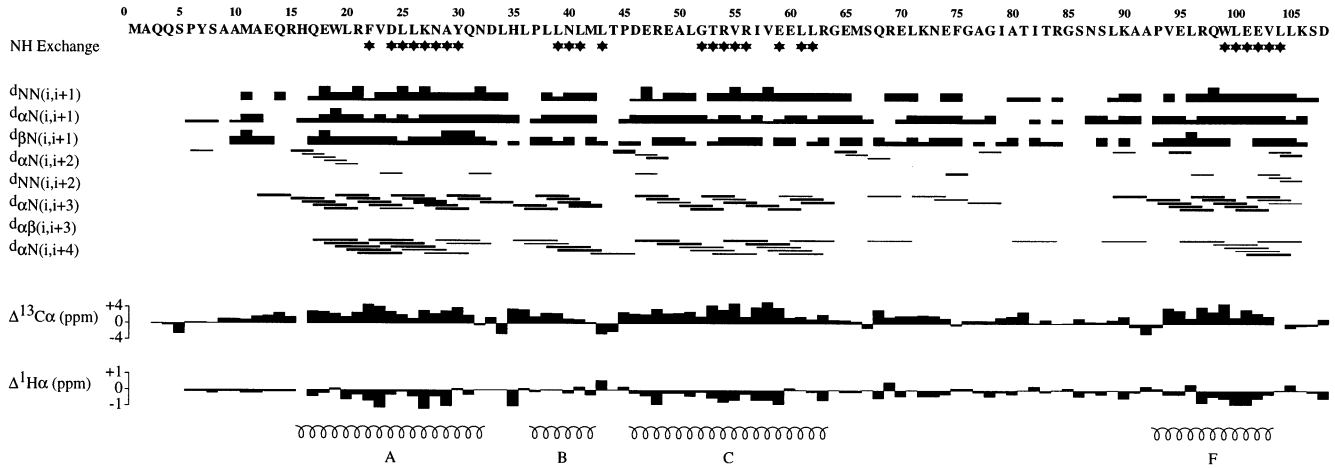

FIGURE 2: Summary of amide exchange data, patterns of sequential and short-range NOEs, and secondary chemical shifts for apo-L75F-TrpR. The protein sequence is indicated on the top row, using the one-letter amino acid code. Filled stars denote residues for which the amide proton exchange time constant is >20 min. NOE connectivities are diagrammed on the next eight rows. The height of the box reflects the intensity of the cross-peak classified as strong (tallest), medium, weak, and very weak (shortest): sequential $d_{NN}(i, i+1)$, $d_{\alpha N}(i, i+1)$, and $d_{\alpha N}(i, i+1)$; short-range $d_{NN}(i, i+2)$, $d_{\alpha N}(i, i+2)$, $d_{\alpha N}(i, i+3)$, $d_{\alpha\alpha}(i, i+3)$, and $d_{\alpha N}(i, i+4)$ are depicted from the first residue involved to the appropriate downstream residue. Differences in parts per million in $^1H_\alpha$ and $^{13}C_\alpha$ chemical shifts relative to random coil values (*35*−*37*) are shown in the rows labeled ΔHα and ΔCα, respectively. The thinnest line corresponds to zero chemical shift difference; residues for which no line is given have not been assigned $^1H_\alpha$ or $^{13}C_\alpha$ chemical shifts. Regions of the protein identified as α-helices by PROCHECK analysis (*33*) are schematically depicted in the last row.

spectrum, for example, cross-peaks with aromatic or upfield-shifted methyl protons (Figure S1 of the Supporting Information).

An ensemble of 40 structures was calculated using the program CNS (*17*), and further refined against NCS restraints with X-PLOR, version 3.1 (*18*). Table 2 summarizes the experimental restraints used in the 3D structure calculations and the statistics for the final set of structures. The 20 structures of lowest conformational energy were selected from this ensemble for use in the structural analysis. The structural statistics for an ensemble of 100 structures were not detectably different from those calculated for the smaller set, indicating that the structure calculations have reached convergence using the available NMR restraints. The average rmsd for backbone atoms of residues 13−108 in the set of 20 apo-L75F-TrpR dimer structures relative to the mean structure is 2.0 Å, and the mean pairwise rmsd for the set is 2.9 ± 0.6 Å. The overall spatial dimensions of the final structures are very similar to those of previously reported TrpR NMR structures (*5*). The distance between the Leu62 C_α atom and the Leu62′ C_α atom, which lie at the C-termini of the C-helices, provides a measure of the size of the dimer core perpendicular to the dimer axis (*5*) and equals 44.2 ± 1.5 Å in apo-L75F-TrpR, compared to the value of 40.5 ± 1.5 Å reported for apo-WT-TrpR (*5*). The distance between the D46 C_α atom and the S86′ C_α atom, which provides an indication of the size of the L-Trp binding pocket, was measured to be 16.9 ± 1.1 Å for apo-L75F-TrpR, within experimental error of the value of 15.4 ± 2.8 Å reported for apo-WT-TrpR. The polypeptide backbone traces of the 15 lowest-energy members of the family of 20 accepted structures superimposed onto the average structure are displayed in Figure 4.

Helical regions in the final 20 structures of apo-L75F-TrpR were defined by Procheck NMR analysis (*33*) and include residues 16−32 (helix A), 37−42 (helix B), 45−63 (helix C), and 93−103 (helix F). Helical trends were observed in the D and E regions of the protein for residues 68−74 and 81−90 as assessed by CSI and the limited set of NOE patterns, although these segments are not defined as helices by Procheck due to the incompleteness of characteristic NOE patterns and the lack of slowly exchanging amides in these regions. Because of this distribution of more versus less well-defined helices in apo-L75F-TrpR, backbone atom rmsds were computed separately for residues 67−92 and for core helices A−C. The average rmsd for backbone atoms was found to be ∼1.0 Å in the dimer core and ∼2.8 Å for residues 67−92 (Table 2). The corresponding values reported for apo-WT-TrpR are 0.9 Å for the A−C dimer core and 3.2 Å for the helix−turn−helix region (*5*). The slightly lower rmsd for residues 67−92 of apo-L75F-TrpR compared to that of apo-WT-TrpR is consistent with the evidence from CSI and NOEs of a less disordered helix−turn−helix domain in the ts mutant than in the wild-type protein. However, both the average and the pairwise rmsd values for residues 67−92 (Table 2) indicate that this part of the apo-L75F-TrpR structure is quite poorly defined relative to the dimer core, as is also true for the apo-WT-TrpR structure (*5*); thus, small differences in average rmsd values may not be significant. Furthermore, for structural calculations that have reached convergence as for apo-L75F-TrpR, the variability within the set of structures reflects the number of NOE restraints, and cannot by itself be taken as an indication of the mobility of residues 67−92. Direct analysis of dynamics is in progress to clarify the origins of the apparent segmental differences within apo-L75F-TrpR.

Given the overall very close similarity between the apo-WT and apo-L75F-TrpR structures, the large number of substantial $^1H-^{15}N$ chemical shift differences between the $^1H-^{15}N$ HSQC spectra of the two proteins (Figure 1 and Table 1) and the unique sets of long-range NOEs observed in the 3D ^{15}N-edited $^1H-^1H$ NOESY spectrum of apo-L75F-TrpR are unexpected. Many of the residues with the largest backbone amide chemical shift differences are near in sequence to residue 75, the site of mutation, suggesting that the ring current expected for the Leu-to-Phe replacement may

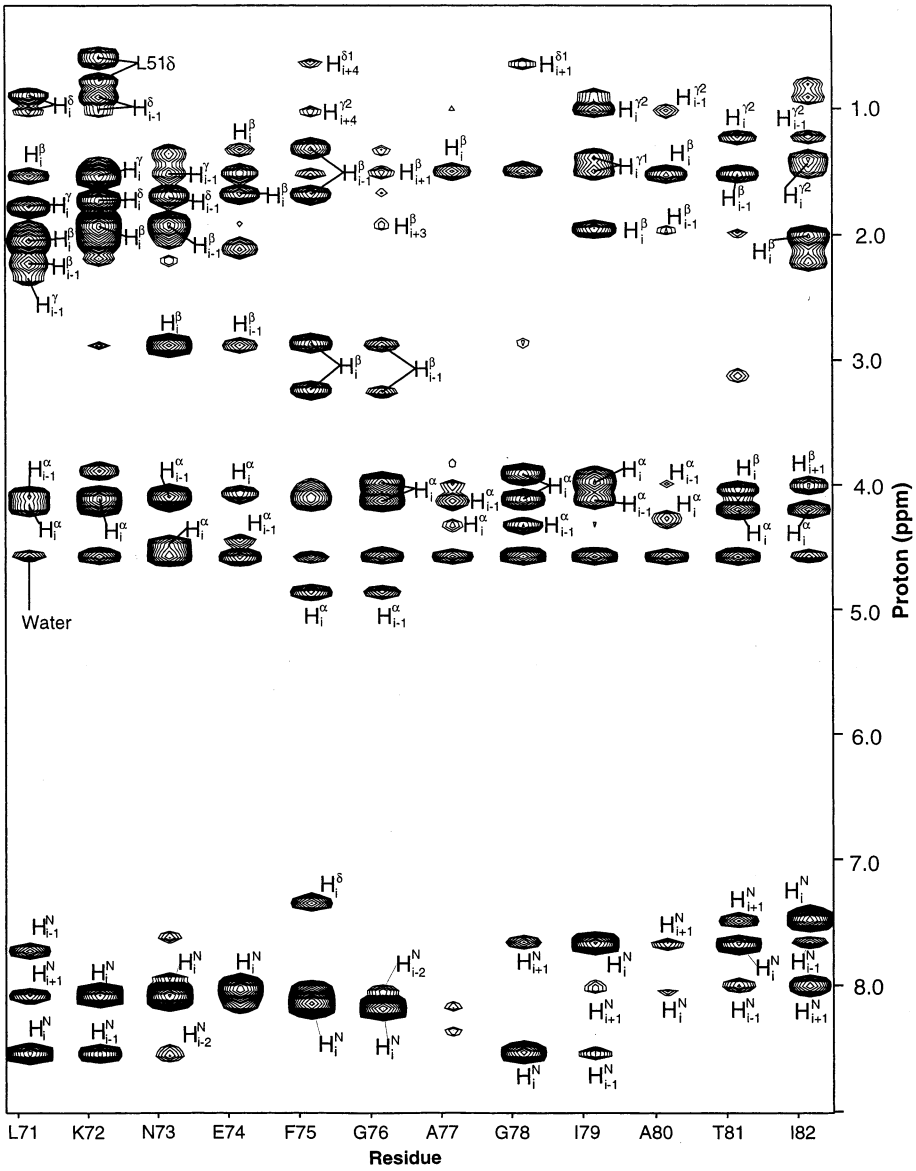

FIGURE 3: Sequential strips extracted from a 3D ^{15}N-edited ^{1}H$-^{1}$H NOESY spectrum of apo-L75F-TrpR. NOE cross-peaks originating from the amides of residues 71−82 are displayed. The plot is a reconstruction, using the *plot_sequence* program (D. Garrett, National Institutes of Health), of ^{15}N planes extracted from the ^{15}N-edited ^{1}H$-^{1}$H NOESY spectrum of apo-L75F-TrpR recorded at 42 °C with an NOE mixing period of 120 ms. Cross-peak partners for each amide and the water signal at 4.58 ppm are marked.

influence their chemical shift. The ring current effect displays a $1/r^3$ distance dependence, and has been reported to be negligible at distances greater than 5.5 Å (*38*). Thus, ring current effects generated by the Leu-to-Phe mutation at position 75 are expected to significantly influence only sites that lie within a relatively short distance. Indeed, some protons of Glu74, Gly76, and Ile79 display weak NOEs to Phe75 ring protons (Figure S2 of the Supporting Information), indicating that their large chemical shift differences can be rationalized by the proximity of the Phe75 ring.

To evaluate local versus long-range origins of the other large chemical shift differences, C_α distances between Phe75 and the affected sites were estimated by inspection of the family of 20 accepted apo-L75F-TrpR structures. Allowing for ring flipping and the uncertainties in side chain positions, we estimated the sphere of influence of the ring current effect to extend up to 10.0 Å from Phe75 C_α. This sphere of influence is *not* meant to imply that ring current effects are isotropic, but rather to provide us with a conservative estimate of the number of residues lying beyond the influence of the F75 ring current effect.

Several of the distances from Phe75 to affected residues are 2−4 times the expected limit of ring current influence (Figure 5), indicating the likelihood that long-range structural perturbations by Phe75 account for the large chemical shift differences in the vicinity of residues Leu43′, Arg56, and Leu89. Interestingly, four of the distantly affected residues (Met42′, Leu43′, Thr44′, and Ala91) lie within a sphere with an approximate radius of 5.0 Å, as determined by examining the family of 20 accepted structures. The center of this sphere is positioned approximately 26.0 Å from Phe75 C_α, suggesting that all four may experience a common, but nonlocal, effect of the mutation. For residues Met66, Ser67, Gln68, Thr81, Ile82, and Thr83, the substantial ^{1}H$-^{15}$N chemical shift changes observed may stem from a combination of local and long-range factors.

The prominent ^{1}H$-^{1}$H cross-peak observed in the unassigned spectrum of apo-L75F-TrpR by Jin et al. (*16*), and

Table 2: Structural Statistics for the Final 20 Accepted NMR Structures of Apo-L75F-TrpR

(A) experimental restraints[a]	
total no. of NOE restraints	769
no. of sequential restraints ($\|i - j\| = 1$)	356
no. of short-range restraints ($1 < \|i - j\| < 4$)	350
no. of long-range restraints ($\|i - j\| > 4$)	24
no. of intersubunit restraints	39
no. of hydrogen bond distance restraints[b]	62
no. of experimental dihedral angle ϕ restraints	68
no. of restraint violations[c]	
distances > 0.3 Å	0
dihedrals > 3°	0
(B) statistics for the calculated structures ({SA}[c])	
deviation from idealized geometry	
bonds (Å)	0.0023 ± 0.0001
angles (deg)	0.54 ± 0.01
impropers (deg)	0.42 ± 0.01
final energies (kcal/mol)	
distance restraints	69.4 ± 6.4
dihedral angles	0.03 ± 0.06
nonbonded (REPEL)[d]	14.6 ± 5.0
root-mean-square deviations	
average atomic rmsd (Å) (dimer)[e]	
backbone atoms[f]	
chain segment of Glu13−Asp108 and Glu13′−Asp108′	2.01
dimer core (helices A−C and A′−C′)[g]	1.04
DNA binding domain (helices D and E, and D′ and E′)[h]	2.64
chain segment of Ser67−Ala92 and Ser67′−Ala92′	2.76
pairwise rmsds (Å) (dimer)[i]	
backbone atoms[f]	
chain segment of Glu13−Asp108 and Glu13′−Asp108′	2.9 ± 0.6
dimer core (helices A−C and A′−C′)[g]	1.5 ± 0.3
DNA binding domain (helices D and E, and D′ and E′)[h]	3.8 ± 1.0
chain segment of Ser67−Ala92 and Ser67′−Ala92′	4.0 ± 1.1

[a] Reported are the total number of unique restraints per monomer. [b] Two distance restraints per hydrogen bond were used. [c] Values are for the ensemble of 20 accepted structures obtained from simulated annealing, {SA}, using CNS (*17*) and further refined with XPLOR (*18*). [d] van der Waals energy function used in the XPLOR algorithm. [e] The average rmsd is the average overall rms difference between the family of structures and the mean structure. [f] N, C_α, C, and O atoms were used for the superposition of backbone coordinates in the rmsd calculations. [g] Dimer core defined as helix A (residues 16−32), helix B (residues 37−42), and helix C (residues 45−63). [h] Helix D (residues 68−74) and helix E (residues 81−90). [i] The pairwise rmsd is the average pairwise rms difference for the family of structures ±1 standard deviation, as defined in ref *18*.

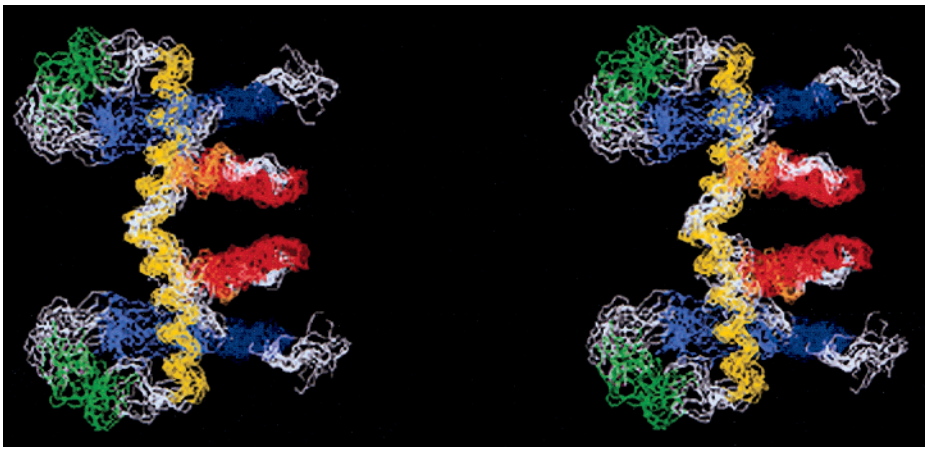

FIGURE 4: Family of accepted apo-L75F-TrpR NMR structures. The stereoview is shown for the overlay of backbone heavy atoms (N, C_α, and C′) of residues 13−108 for 15 of the 20 lowest-energy structures relative to the mean structure, and was generated with MOLMOL software (*34*). Residues in helix A (16−32) are colored red, thpse in helix B (37−42) orange, those in helix C (45−63) yellow, those in helix D (68−74) green, those in helix E (81−90) blue, and those in helix F (93−103) indigo. Other chain segments are white. Disordered residues (1−12) of the N-terminus are omitted for clarity.

attributed to slowly exchanging amide protons unique to the mutant protein, is here verified to arise from the $d_{NN}(i, i + 1)$ connectivity between the amides of residues Met42 and Leu43. Residues 42 and 43 are among those that display significant chemical shift differences from apo-WT-TrpR (Table 1), but lie well outside the sphere of influence of the F75 ring current (Figure 5). The strong interaction between the Met42 and Leu43 amide protons, and/or the structural changes that it reflects, could provide an explanation for the large chemical shift changes observed for residues in this region of the mutant protein relative to wild type (Table 1). The chemical shift perturbations observed in apo-L75F-TrpR for Leu43, whose methyl protons show NOEs to ring protons of Trp19 in both wild-type and mutant proteins,

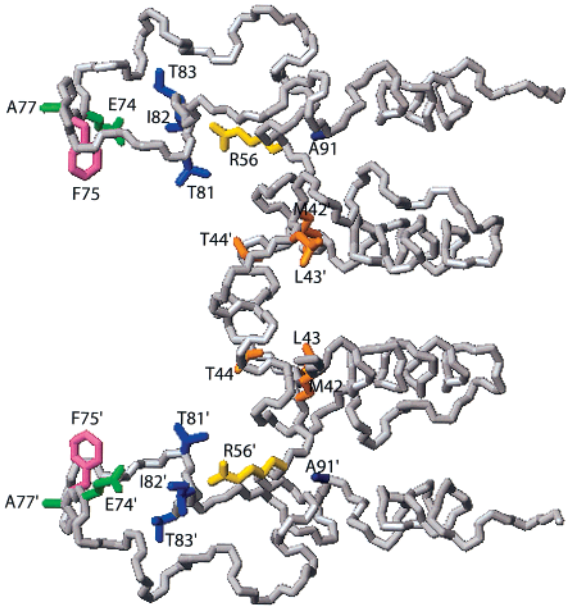

FIGURE 5: Backbone trace of the energy-minimized average structure of apo-L75F-TrpR. Positions of residues Met42, Leu43, and Thr44 (orange), Arg56 (yellow), Thr81, Ile82, and Thr83 (blue), Ala91 (indigo), and Phe75 (pink) are indicated. Selected C_α distances from Phe75 were estimated on the family of 20 accepted apo-L75F-TrpR structures to be 21.9 ± 2.2 Å for Met42′, 24.1 ± 2.3 Å for Leu43′, 22.8 ± 2.3 Å for Thr44′, 18.0 ± 1.8 Å for Arg56, 5.6 ± 0.6 Å for Ala77, and 26.3 ± 2.4 Å for Ala91.

suggest that the fluorescence differences noted by Jin et al. (*16*) are likely due to an altered environment for Trp19. Consistent with this interpretation, large chemical shift differences are noted for Trp19 and for residues Val23, Leu26, and Tyr30, which all lie on one "face" of helix A.

In addition, a prominent 9.15 ppm−114.2 ppm cross-peak in the $^1H-^{15}N$ HSQC spectrum of apo-L75F-TrpR is not observed in the spectrum of apo-WT-TrpR (Figure 1). This cross-peak is here assigned unambiguously to the amide of Thr44, located just before the N-terminal end of helix C. The T44 resonance is one of four that are observed in the HSQC spectrum of apo-L75F-TrpR but not in the corresponding spectrum of apo-WT-TrpR at pH 5.7 (Figure 1). In the HSQC spectrum of apo-WT-TrpR at pH 6.05, Finucane and Jardetzky (*11*) observed the NH resonance of T44 at ∼9.15 (^1H) and ∼115 ppm (^{15}N). The other three resonances (Arg84, Gly85, and Ser88) missing from the WT spectrum under our solution conditions are not reported in the literature for apo-WT-TrpR (*8*, *11*). The disappearance of the Thr44 signal may reflect a chemical exchange process present in apo-WT-TrpR at pH 5.7 but not occurring on the same time scale at pH 6.05 or in apo-L75F-TrpR at pH 5.7.

The structural alteration in the B−C turn region may likewise be reflected in the larger Leu62−Leu62′ distance in apo-L75F-TrpR compared to that in apo-WT-TrpR, as the turn could act as a fulcrum governing the distance between the carboxyl ends of the C-helices. Furthermore, the B−C turn region forms part of the binding pocket for L-Trp. In apo-WT-TrpR, the carbonyl oxygens of Asn40, Leu41, and Leu43 accept hydrogen bonds from the guanidino group of Arg84 (*3*). In holo-WT-TrpR, the α-amino group of L-Trp displaces the guanidino group of Arg84 (*2*). The structural changes detected in the B−C turn may thus be related to the altered L-Trp binding of the mutant protein (*16*).

Such significant structural changes so far distant from the site of mutation directly indicate the long-range nature of the effects of the Leu75-to-Phe substitution within the context of an otherwise very similar fold. The present case is especially intriguing because of the conservative nature of the replacement and the solvent-exposed location of the residue position. These results serve as important reminders of the inherent cooperativity of protein systems and the consequent inability to directly interpret changes in properties that result from changes in sequence. The effects of the L75F mutation (*16*) on protein stability, L-Trp binding, and DNA binding in vitro, and on temperature sensitivity in vivo, cannot be ascribed directly to the new side chain identity, or to other local changes. Furthermore, despite the available structural detail on both mutant and wild-type proteins, the mechanisms responsible for the distant structural changes are not clear. However, Arg84 of the ligand binding pocket follows helix E residues 81−83, which are strongly affected by the mutation, suggesting its involvement in the long-range propagation of the observed effects.

TrpR is an unusual protein in many respects, not the least of which are its structure and dynamics. Its fold depends on the complete interdependence of secondary, tertiary, and quaternary levels of structural organization, as inferred from the two-state unfolding transition of folded dimers to unstructured monomers (*39*). The dimer is extraordinarily stable with a thermal denaturation midpoint of >90 °C (*40*), but exhibits extensive dynamic disorder at room temperature in its DNA binding site, the helix−turn−helix domain (*8*−*10*, *12*). The dynamics of this domain of the protein are thermodynamically coupled to binding of the L-Trp and DNA ligands (*41*), with consequences for both the affinity and specificity of ligand recognition (*15*, *41*−*43*). Given the important role of dynamics in both the function and structure of TrpR, it would come as no surprise if the effects of the L75F mutation can be further understood through analysis of protein dynamics.

ACKNOWLEDGMENT

The NMR experiments were carried out at Montana State University on a DRX600 spectrometer, purchased in part with funds from the NIH shared instrumentation grant program (SIG Grant 1-S10RR13878-01), and the NSF-EPSCOR program for the State of Montana. We thank Dr. Dwight Schwartz for computer support, June Wong Fukayama (Princeton University) for her help with protein expression and purification, and Rob Fairman (Haverford College, Haverford, PA) for ultracentrifugal analysis. R.T. gratefully acknowledges Dr. Mahesh Jaseja for assistance with NMR data processing using the Xwinnmr Bruker Inc. software and for productive discussions regarding NMR data analyses. We thank Professor Ann McDermott (Columbia University, New York, NY) for productive discussions about ring current effects and for critical review of the manuscript.

SUPPORTING INFORMATION AVAILABLE

NMR experiments and parameters used to acquire chemical shift assignments and structural restraints (Table S1), chemical shift assignments for apo-L75F-TrpR (Table S2), and $^1H-^1H$ chemical shifts (Figures S1 and S2). This material is available free of charge via the Internet at http://pubs.acs.org.

REFERENCES

1. Joachimiak, A., Kelley, R. L., Gunsalus, R. P., Yanofsky, C., and Sigler, P. B. (1983) *Proc. Natl. Acad. Sci. U.S.A. 80*, 668−672.
2. Schevitz, R. W., Otwinowski, Z., Joachimiak, A., Lawson, C. L., and Sigler, P. B. (1985) *Nature 317*, 782−786.
3. Zhang, R. G., Joachimiak, A., Lawson, C. L., Schevitz, R. W., Otwinowski, Z., and Sigler, P. B. (1987) *Nature 327*, 591−597.
4. Arrowsmith, C., Pachter, R., Altman, R., and Jardetzky, O. (1991) *Eur. J. Biochem. 202*, 53−66.
5. Zhao, D., Arrowsmith, C. H., Jia, X., and Jardetzky, O. (1993) *J. Mol. Biol. 229*, 735−746.
6. Zhang, H., Zhao, D., Revington, M., Lee, W., Jia, X., Arrowsmith, C., and Jardetzky, O. (1994) *J. Mol. Biol. 238*, 592−614.
7. Sigler, P. B. (1992) *Transcriptional regulation*, Cold Spring Harbor Laboratory Press, Plainview, NY.
8. Czaplicki, J., Arrowsmith, C., and Jardetzky, O. (1991) *J. Biomol. NMR 1*, 349−361.
9. Zheng, Z., Czaplicki, J., and Jardetzky, O. (1995) *Biochemistry 34*, 5212−5223.
10. Gryk, M. R., Finucane, M. D., Zheng, Z., and Jardetzky, O. (1995) *J. Mol. Biol. 246*, 618−627.
11. Finucane, M. D., and Jardetzky, O. (1995) *J. Mol. Biol. 253*, 576−589.
12. Schmitt, T. H., Zheng, Z., and Jardetzky, O. (1995) *Biochemistry 34*, 13183−13189.
13. Gryk, M. R., and Jardetzky, O. (1996) *J. Mol. Biol. 255*, 204−214.
14. Reedstrom, R. J., and Royer, C. A. (1995) *J. Mol. Biol. 253*, 266−276.
15. Gryk, M. R., Jardetzky, O., Klig, L. S., and Yanofsky, C. (1996) *Protein Sci. 5*, 1195−1197.
16. Jin, L., Fukayama, J. W., Pelczer, I., and Carey, J. (1999) *J. Mol. Biol. 285*, 361−378.
17. Brunger, A. T., Adams, P. D., Clore, G. M., DeLano, W. L., Gros, P., Grosse-Kunstleve, R. W., Jiang, J. S., Kuszewski, J., Nilges, M., Pannu, N. S., Read, R. J., Rice, L. M., Simonson, T., and Warren, G. L. (1998) *Acta Crystallogr. D54* (Part 5), 905−921.
18. Brunger, A. T. (1992) *X-PLOR version 3.1, A System for X-ray Crystallography and NMR*, Yale University Press, New Haven, CT.
19. Marion, D., Ikura, M., Tschudin, R., and Bax, A. (1989) *J. Magn. Reson. 85*, 393−399.
20. Delaglio, F., Grzesiek, S., Vuister, G. W., Zhu, G., Pfeifer, J., and Bax, A. (1995) *J. Biomol. NMR 6*, 277−293.
21. Garrett, D. S., Powers, R., Gronenborn, A. M., and Clore, G. M. (1991) *J. Magn. Reson., Ser. B 95*, 214−220.
22. Bodenhausen, G., and Ruben, D. J. (1980) *Chem. Phys. Lett. 69*, 185−189.
23. Shaka, A. J., Keeler, J., and Freeman, R. (1983) *J. Magn. Reson. 53*, 313−340.
24. Grzesiek, S., and Bax, A. (1992) *J. Am. Chem. Soc. 114*, 6291−6293.
25. Grzesiek, S., and Bax, A. (1992) *J. Magn. Reson. 99*, 201−207.
26. Grzesiek, S., and Bax, A. (1993) *J. Biomol. NMR 3*, 185−204.
27. Grzesiek, S., Anglister, J., and Bax, A. (1993) *J. Magn. Reson. 101*, 114−119.
28. Shaka, A. J., Lee, C. J., and Pines, A. (1988) *J. Magn. Reson. 77*, 274−293.
29. Marion, D., Kay, L. E., Sparks, S. W., Torchia, D. A., and Bax, A. (1989) *J. Am. Chem. Soc. 111*, 1515−1517.
30. Kay, L. E., Marion, D., and Bax, A. (1989) *J. Magn. Reson. 84*, 72−84.
31. Bax, A., Clore, G. M., Driscoll, P. C., Gronenborn, A. M., and Ikura, M. (1990) *J. Magn. Reson. 87*, 620−627.
32. Stein, E. G., Rice, L. M., and Brunger, A. T. (1997) *J. Magn. Reson. 124*, 154−164.
33. Laskowski, R. A., Rullmann, J. A. C., MacArthur, M. W., Kaptein, R., and Thornton, J. M. (1996) *J. Biomol. NMR 8*, 477−486.
34. Koradi, R., Billeter, M., and Wuthrich, K. (1996) *J. Mol. Graphics 14*, 51−52.
35. Wishart, D. S., Bigam, C. G., Yao, J., Abildgaard, F., Dyson, H. J., Oldfield, E., Markley, J. L., and Sykes, B. D. (1995) *J. Biomol. NMR 6*, 135−140.
36. Wishart, D. S., and Sykes, B. D. (1994) *J. Biomol. NMR 4*, 171−180.
37. Wishart, D. S., and Nip, A. M. (1998) *Biochem. Cell Biol. 76*, 153−163.
38. Case, D. A. (1995) *J. Biomol. NMR 6*, 341−346.
39. Gittelman, M. S., and Matthews, C. R. (1990) *Biochemistry 29*, 7011−7020.
40. Chou, W. Y., and Matthews, K. S. (1989) *J. Biol. Chem. 264*, 18314−18319.
41. Jin, L., Yang, J., and Carey, J. (1993) *Biochemistry 32*, 7302−7309.
42. Carey, J., Lewis, D. E., Lavoie, T. A., and Yang, J. (1991) *J. Biol. Chem. 266*, 24509−24513.
43. Szwajkajzer, D., and Carey, J. (1997) *Biopolymers 44*, 181−198.

BI020304T